ACS APPLIED MATERIALS & INTERFACES
Research Article
www.acsami.org

Engineering the Interface Characteristics of Ultrananocrystalline Diamond Films Grown on Au-Coated Si Substrates

Kamatchi Jothiramalingam Sankaran,[†] Kalpataru Panda,[§] Balakrishnan Sundaravel,[§] Huang-Chin Chen,[‡] I-Nan Lin,[‡] Chi-Young Lee,[†] and Nyan-Hwa Tai*,[†]

[†]Department of Materials Science and Engineering, National Tsing-Hua University, Hsinchu 300, Taiwan, Republic of China
[§]Materials Science Group, Indira Gandhi Centre for Atomic Research, Kalpakkam 603 102, India
[‡]Department of Physics, Tamkang University, Tamsui 251, Taiwan, Republic of China

ABSTRACT: Enhanced electron field emission (EFE) properties have been observed for ultrananocrystalline diamond (UNCD) films grown on Au-coated Si (UNCD/Au−Si) substrates. The EFE properties of UNCD/Au−Si could be turned on at a low field of 8.9 V/μm, attaining EFE current density of 4.5 mA/cm^2 at an applied field of 10.5 V/μm, which is superior to that of UNCD films grown on Si (UNCD/Si) substrates with the same chemical vapor deposition process. Moreover, a significant difference in current−voltage curves from scanning tunneling spectroscopic measurements at the grain and the grain boundary has been observed. From the variation of normalized conductance $(dI/dV)/(I/V)$ versus V, bandgap of UNCD/Au−Si is measured to be 2.8 eV at the grain and nearly metallic at the grain boundary. Current imaging tunneling spectroscopy measurements show that the grain boundaries have higher electron field emission capacity than the grains. The diffusion of Au into the interface layer that results in the induction of graphite and converts the metal-to-Si interface from Schottky to Ohmic contact is believed to be the authentic factors, resulting in marvelous EFE properties of UNCD/Au−Si.

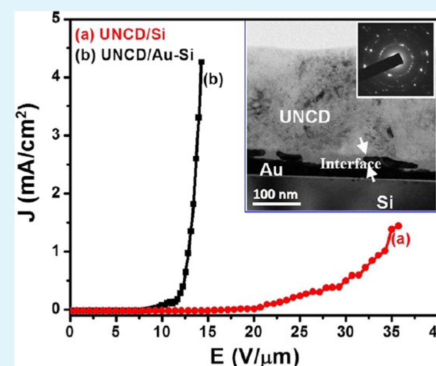

KEYWORDS: *ultrananocrystalline diamond films, Au-interface layer, nanographite, electron field emission, high resolution transmission electron microscopy, scanning tunneling spectroscopy*

■ INTRODUCTION

Electrons from cold cathode emitters are usually obtained by applying an electric field, which tunnels the electrons from the material surface into vacuum.[1−4] Materials like semiconductor nanowires or nanotubes, carbon nanotubes, and diamond thin films have been reported to exhibit low turn-on voltages and high current densities, making them suitable for cold cathode emitter applications. Potentially, these materials can be used in display technologies such as field emission displays (FED).[5−9] Among such likely materials, the unique physical and chemical properties, high thermal conductivity, and a surface with negative electron affinity (NEA) make diamond a more promising material for applications in FED devices.[9−16] A special form of diamond, ultrananocrystalline diamond (UNCD) film, which possesses ultrasmall grain sizes of 2−5 nm and realizes very smooth film surfaces, has recently captured broad interest because of its superb electron field emission (EFE) behavior compared to that of micrometer-sized diamond films.[17,18] The grains in UNCD films consist of sp^3 carbon phases while the grain boundaries contain sp^2 carbon phases. The smallness in crystal sizes and the abundance of sp^2 phases make these materials useful for electron field emitter applications.[19−21]

Apart from the combined role of all intrinsic characteristics of diamond, the diamond-to-substrate interface also affects the electron field emission (EFE) behavior significantly. Such interface effects can also noticeably influence other properties of the diamond films. Mandal et al.[22] reported about the charges trapped in the interface of the diamond-like carbon films on Si substrate, which contributed to modifying various electrical and optical properties, while Xu et al.[23] explored the importance of the NEA and graphitic inclusions in CVD diamond such as electrons being accelerated toward the film−substrate interface and escaping into vacuum. Higher nucleation site density helps in the evolution of electron emission centers. Obtaining textured, continuous, adherent, and smooth diamond films using methods like in situ carburization, bias enhanced nucleation, and the two stage nucleation process as well as substrate pretreatment and seeding processes have been reported to increase the number of nucleation sites and enhance EFE properties.[24−33] Altering the carbon layer content, deposition of metallic layers such as Ti, Cr, Mo, or dual metal layers like W−Al or pretreatment with Ti powder on Si substrates, also enabled one to obtain high nucleation densities and enhanced EFE properties.[34−41] Improvement of the EFE properties in diamond films grown on Au-coated Si substrates

Received: May 18, 2012
Accepted: July 23, 2012
Published: July 23, 2012

ACS Publications © 2012 American Chemical Society

was attributed to reduction of conduction barrier of electron transport from the substrates to the diamond surface.[42,43]

In this paper, we engineered the interface characteristics of UNCD films using Au-interlayer and markedly enhanced the EFE properties of the films. We reported an in-depth investigation on the consequence of Au-coatings on the microstructural evolution of the film's interface characteristics using transmission electron microscopy (TEM) and scanning tunneling microscopy (STM). The scanning tunneling spectroscopy (STS) has been used to determine potential electron emission sites. The possible mechanism that prompts the Au-coating to enhance the EFE properties of UNCD films is discussed.

■ EXPERIMENTAL METHODS

In this work, 100 nm Au was deposited on n-type Si substrates by a dc sputter deposition system (Helix) using a power of 50 W in argon partial pressure of 5 mTorr. Prior to Au deposition, a thin layer of Cr (~5 nm) was deposited on Si to achieve strong adhesion of Au on Si. The bare Si and Au-coated Si substrates were ultrasonicated for 45 min in methanol solution containing the mixture of diamond powder (about 4 nm in size) and Ti powder (SIGMA-Aldrich) (365 mesh) to facilitate the nucleation process. The Au coatings were adhered strongly on the Si substrates even after the ultrasonication process due to the presence of Cr-interlayer between Au and Si. UNCD films were deposited by a microwave plasma enhanced chemical vapor deposition system (IPLAS, Cyrannus) using Ar(99%)/CH_4(1%) gas at 1200 W and 120 Torr for 3 h. The growth process was carried out at low temperatures (<475 °C) without any intentional heating of the substrate. UNCD films deposited on bare Si substrates are designated as "UNCD/Si", and UNCD films deposited on Au-coated Si are designated as "UNCD/Au−Si".

The EFE characteristics of the samples were measured using a parallel plate configuration, where a molybdenum rod with a diameter of 2 mm was used as anode. The current density versus electrical field (J−E) characteristics were acquired using Keithley 237 electrometer, and the EFE behavior of materials was explained using the Fowler Nordheim (FN) theory.[44] The turn-on field (E_0)was designated as the interception of the straight lines extrapolated from the low field and high field segments of the FN plots, viz., $\log(J/E^2) - 1/E$. The local EFE behavior was investigated using an ultra high vacuum scanning tunneling microscope (STM, 150 Aarhus, SPECS GmbH) operated in the temperature range of 90−400 K and at a base pressure of 10^{-10} mbar, whereas the scanning tunneling spectroscopy (STS) was performed during scanning, and the data presented here are the average of many reproducible spectra acquired in subsequent scans to evaluate the local density of states (LDOS). The tunneling tips were prepared by electrochemical etching of tungsten tips. The imaging was performed with a set current of 0.59 nA and with a relatively high bias voltage between −2.5 and +3.5 V. The current imaging tunneling spectroscopy (CITS) mode in STM was utilized to correlate STM images with the surface LDOS distribution. CITS involves acquiring, simultaneously with the constant−current topography, I−V curve, the measurement with the feedback loop off, in every point of the surface. Hall measurements were carried out in a van der Pauw configuration (ECOPIA HMS-3000) to examine the conducting behavior of the films. The crystalline quality and the depth profile of the UNCD films was characterized by Raman spectroscopy (Lab Raman HR800, Jobin Yvon; λ = 632 nm) and secondary ions mass spectroscopy (SIMS; Cameca IMS-4f), respectively. High resolution transmission electron microscopy (HRTEM; JEOL-2100F) was examined to characterize the microstructures of the UNCD films.

■ RESULTS AND DISCUSSION

The UNCD film's thicknesses on Si and Au-coated Si are about 450 and 330 nm, respectively, which were estimated from cross-sectional field emission scanning electron microscopic (FESEM, JEOL-6200) images (not shown). The presence of Au-coating does not markedly influence the surface morphology of the UNCD films. Figures that were not shown here indicate that both UNCD/Si and UNCD/Au−Si films contain ultrasmall granular structure with a very smooth surface. However, Figure 1 illustrated that the utilization of Au-coating

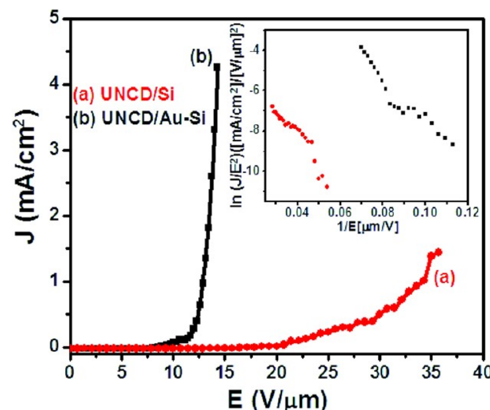

Figure 1. Electron field emission properties of (a) UNCD/Si (solid circles) and (b) UNCD/Au−Si films (solid squares). The inset is the Fowler Nordheim plot of the corresponding data.

as interlayer markedly altered the EFE properties of UNCD films. The inset of Figure 1 is the FN plot of the corresponding field emission data, from which the E_0 for the EFE process was estimated. Interestingly, the Au interlayer significantly enhances the EFE properties of the UNCD films. While the EFE behavior of the UNCD/Si films was turned on at $(E_0)_{\mathrm{UNCD/Si}}$ = 18.6 V/μm and attained an electron emission current density of $(J_e)_{\mathrm{UNCD/Si}}$ = 1.4 mA/cm^2 at the applied field of 35.5 V/μm (curve a), the UNCD/Au−Si films can be turned on at a markedly lower field, $(E_0)_{\mathrm{UNCD/Au-Si}}$ = 8.9 V/μm, with pronounced larger EFE current density, $(J_e)_{\mathrm{UNCD/Au-Si}}$ = 4.5 mA/cm^2 under 10.5 V/μm field strength (curve b). The values are tabulated in Table 1. Moreover, the effective work functions

Table 1. Electron Field Emission Properties of the UNCD Films Deposited on Si and Au-coated Si Substrates

materials	turn-on field (V/μm)	current density (mA/cm^2)	effective work function (eV)
UNCD/Au−Si	8.9	4.5 @ 10.5 V/μm	0.0148
UNCD/Si	18.6	1.4 @ 35.5 V/μm	0.0195

of these UNCD films calculated from the slope of the FN plots were $\Phi_{\mathrm{UNCD/Si}}$ = 0.0195 eV and $\Phi_{\mathrm{UNCD/Au-Si}}$ = 0.0148 eV. The Hall measurements in van der Pauw configuration indicates that the UNCD/Au−Si films are of high conductivity (σ = 0.74 (Ω-cm)$^{-1}$) with sheet carrier concentration of 6.61 × 10^{20} cm^{-2}. The resistivity of the UNCD/Si films is too large to be measured by van der Pauw configuration. These results indicate clearly that the enhancement on the EFE properties for the UNCD/Au−Si films is closely related to the improvement in the electrical properties of the films due to the utilization of Au-coating as interlayer.

For the purpose of understanding the nature of the emission sites that enhance the EFE properties of the UNCD/Au−Si films, in comparison with UNCD/Si, the local electrical properties of the films are investigated by STS. Notably,

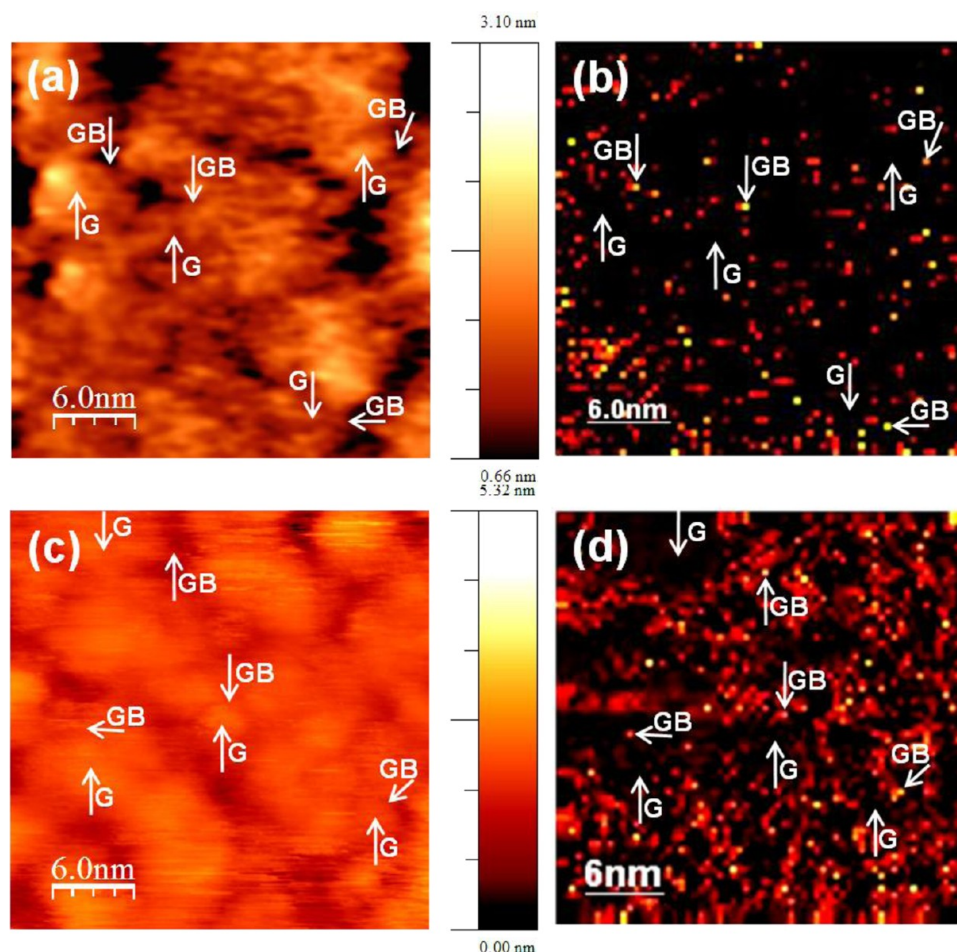

Figure 2. (a) UHV STM and (b) CITS images of UNCD/Si films; (c) UHV STM and (d) corresponding CITS images of UNCD/Au−Si films, showing that the UNCD/Au−Si films contain more abundant electron emitting sites. The typical grains and grain boundaries are marked as "G" and "GB", respectively.

UNCD/Si is highly resistive and STS measurements could not be performed in this sample. Only after sputtering under Ar environment for 1 min the UNCD/Si films become conducting and then STS measurements were done. In contrast, UNCD/Au−Si films have inherently high electrical conductivity for STS measurements. Figure 2a shows the high resolution STM image of UNCD/Si after 1 min of Ar sputtering. The grain size is between 3 and 6 nm, and the root-mean-square (rms) roughness is found to be 0.7 nm. The typical grains and grain boundaries are marked as "G" and "GB", respectively. Figure 2b shows the CITS image corresponding to Figure 2a taken at a sample bias of −3.0 V. Bright and dark regions in CITS image are visible with their shapes having similarity with the shapes of GB and G of the STM image in Figure 2a, respectively. The CITS image (Figure 2b) shows clearly that the electrons are mainly emitted from the grain boundaries (bright regions) rather than grains. Figure 2c shows the high resolution STM image of UNCD/Au−Si. The grain size is 3−5 nm, and the rms roughness is found to be 0.5 nm. The CITS image taken at a sample bias of −3.25 V corresponding to Figure 2c is shown in Figure 2d. The CITS image reveals again that the GBs are the prominent electron emission sites in comparison to that of the grains. Moreover, in comparison with the CITS image of UNCD/Si (Figure 2b), it is clearly evident that the emission sites (bright regions) are more abundant for UNCD/Au−Si (Figure 2d). Such an observation is in accord with the enhanced EFE behavior for the UNCD films grown on Au−Si substrates (Figure 1).

For the characterization of the local electronic properties of the UNCD/Si and UNCD/Au−Si films, *I*−*V* curves were taken from STS at various positions of grains and grain boundaries (Figure 3) in the STM images shown in Figure 2a,c. Only the negative portion of the *I*−*V* curves, which represents the emission of electrons from the samples, is shown here. We observe a significant difference in the *I*−*V* characteristic curve at the grain and grain boundary for both the samples. The UNCD/Au−Si sample (curves a and b) emits better than the UNCD/Si sample (curves c and d). The grain boundaries in both the samples (curves a and c) emit electrons at a lower E_0 compared to the grains (curves b and d), consistent with the CITS images shown in Figure 2b,d. Additionally, for UNCD/Au−Si films, at the sample voltage of 2.0 V, grain boundaries (curve a) acquire a good tunneling current of ∼60 nA whereas the grains (curves b) exhibit a relatively low tunneling current (∼16 nA). Both the grains and grain boundaries for the UNCD/Si films emit an insignificant amount of tunneling current at such a low voltage.

We deduce the surface LDOS[45,46] for understanding the mechanism that alters the EFE properties of these UNCD films. The *I*−*V* characteristic curves of STS measurements shown in Figure 3 are used to calculate the normalized derivative of multiple averaged spectra, the normalized conductance (*dI*/

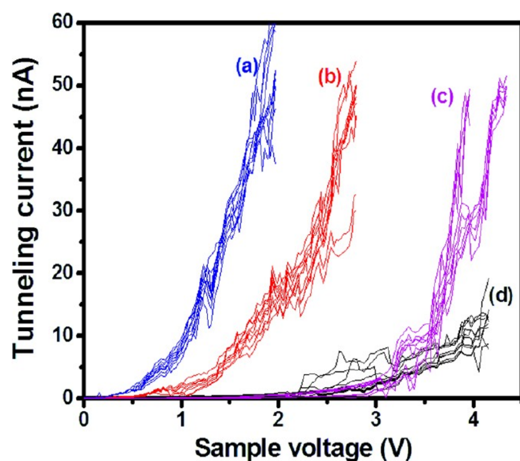

Figure 3. $I-V$ curves in STS measurements at the (a) grain boundary and (b) grain of UNCD/Au−Si films; those at the (c) grain boundary and (d) grain of UNCD/Si films, showing that the UNCD/Au−Si films emit better than the UNCD/Si films and grain boundaries emit better than the grains.

$dV)/(I/V)$ at the grain, and the grain boundary of the UNCD/Au−Si and UNCD/Si films. The singularity in the bandgap region was removed using an average value for I/V, which is nonzero. The normalized conductance corresponding to these locations are plotted in Figure 4a,b for UNCD/Si and UNCD/Au−Si, respectively. From the variation of normalized conductance $(dI/dV)/(I/V)$ versus V for UNCD/Si films, shown in Figure 4a, the bandgap is estimated to be 4.7 eV at the UNCD grain from spectrum (i) and 3.9 eV at the grain boundary from spectrum (ii) for UNCD/Si. Intermediate states are not seen in the bandgap. The estimated band gap is in accord with the theoretical band gap value of 4.2 eV for nanodiamond.[47−49,53] Moreover, we obtained a bandgap of about 2.8 eV on the UNCD grain from the spectrum (iii) (Figure 4b) for the UNCD/Au−Si; this is smaller than 4.7 eV for UNCD/Si (Figure 4a). Furthermore, a bandgap of grain boundary shows metallic behavior (spectrum (iv), Figure 4b). These observations are in accord with the CITS examinations (Figure 2b,d), where we observe that the grain boundaries are the prominent field emitters. Hence, the Au interlayer would have a significant role on altering the grain boundary characteristics that enhances the EFE behavior of UNCD films, which will be further discussed in detail shortly.

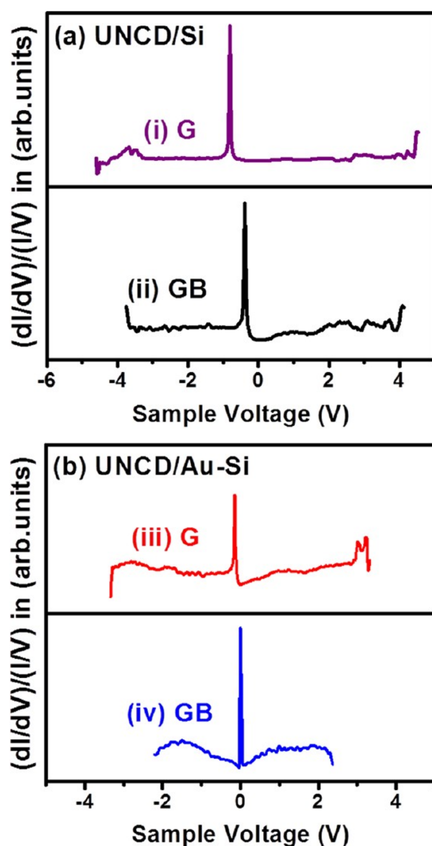

Figure 4. (a) Normalized differential conductance $(dI/dV)/(I/V)$ at the (i) grains (G) and (ii) grain boundaries (GB) of UNCD/Si films; (b) $(dI/dV)/(I/V)$ at (iii) grains (G) and (iv) grain boundaries (GB) of UNCD/Au−Si films. Each spectrum is averaged over 10 scanned spectra, shown in Figure 3.

The Raman spectroscopy is a convenient technique to investigate diamond or related materials. Figure 5 shows the Raman spectra of (a) UNCD/Si and (b) UNCD/Au−Si substrates that were deconvoluted using the multipeak Lorentzian fitting method. Figure 5a shows that, for UNCD/Si films, there exist Raman resonance peaks at around 1160 cm^{-1} and 1465 cm^{-1} attributing, respectively, to the ν_1 and ν_3 modes of trans-polyacetylene (trans-PA) present in the grain boundaries of UNCD films.[50] A broadened peak around 1310 cm^{-1} (designated as D-band), which corresponds to the disordered sp^2 bonded carbon, is observed for these UNCD films.[51] The sharp Raman peak at 1332 cm^{-1}, which is commonly observed for the diamond films with micrometer-sized grains, is not observed in UNCD using visible Raman spectroscopy, as Raman resonance is more sensitive to sp^2 sites, as compared with that to sp^3 bonds.[52] The G-band of the UNCD films is observed at 1538 cm^{-1}. The shifting in the G-band resonance peak occurs due to the smallness in grain size and the presence of growth defects.[50] A shoulder peak around 1600 cm^{-1} (designated as G□-band) is seen, that possibly arises from the nanocrystalline graphitic content in the films.[52] Figure 5b shows that the Raman spectrum of the UNCD films grown on Au−Si substrates is basically the same as those for the UNCD/Si films without the Au-interlayer. It shows slightly higher intensities of D and G peaks, indicating amorphization

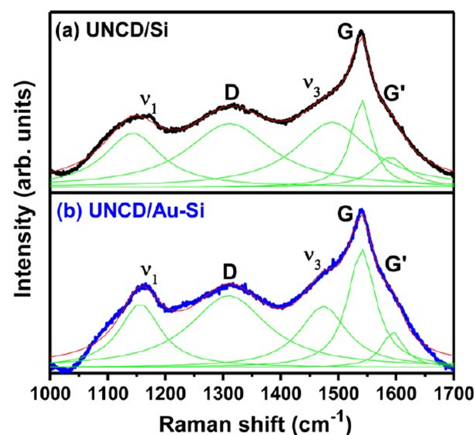

Figure 5. Raman spectra of (a) UNCD/Si films and (b) UNCD/Au−Si films. The Raman spectra are deconvoluted using the multipeak Lorentzian fitting method.

and graphitization type of transitions.[53] The Raman spectra show I_D/I_G values (ratio of intensities of D-peak to G-peak) of 0.74 and 0.92 for UNCD/Si and UNCD/Au−Si substrates, respectively. The G-peaks are found to be at 1538 and 1540 cm^{-1} for UNCD/Si and UNCD/Au−Si substrates, respectively. The increase of the I_D/I_G value from 0.74 to 0.92 and G-band shift to higher wavenumber implies the formation of nanographite and decrease in sp^3 content from *a*-C according to a three-stage model of increasing disorder in carbon materials;[52,54] i.e., there is conversion of sp^3 to sp^2 content due to the presence of Au-interlayer. The depth profiles of these corresponding samples are examined using SIMS so as to understand the interfacial characteristics of UNCD/Si and UNCD/Au−Si films. The depth profile of Si (Figure 6a) clearly

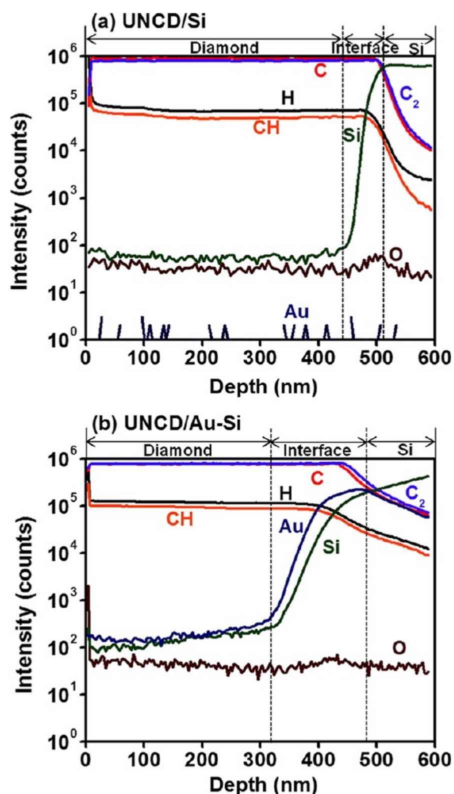

Figure 6. SIMS depth profiles of C, C_2, CH, Au, Si, H, and O species in (a) UNCD/Si films and (b) UNCD/Au−Si films, showing that Au-interlayer interdiffused with the Si markedly.

shows that there is diffusion of Si in the interfacial (*a*-C) layer, but the diffusion of Si on UNCD is not clearly observed. In contrast, the depth profile of UNCD/Au−Si in Figure 6b clearly shows that there are pronounced Au- and Si-ion counts observed in the interface layer, inferring the marked diffusion of Au (Si) species into the interface layer. The Au (Si) counts drop abruptly to a level lower than the detection limit in the diamond layer.

The Raman spectra and SIMS cannot clearly account for the source of modification on the EFE behavior for UNCD films due to Au-coatings. TEM microstructural investigation is needed for better understanding the genuine factor that influences the EFE behavior of the UNCD films. Figure 7a shows the plane-view TEM micrograph of UNCD/Si films, indicating that UNCD films contain very small grains (∼5 nm), which are uniformly distributed. The corresponding selective

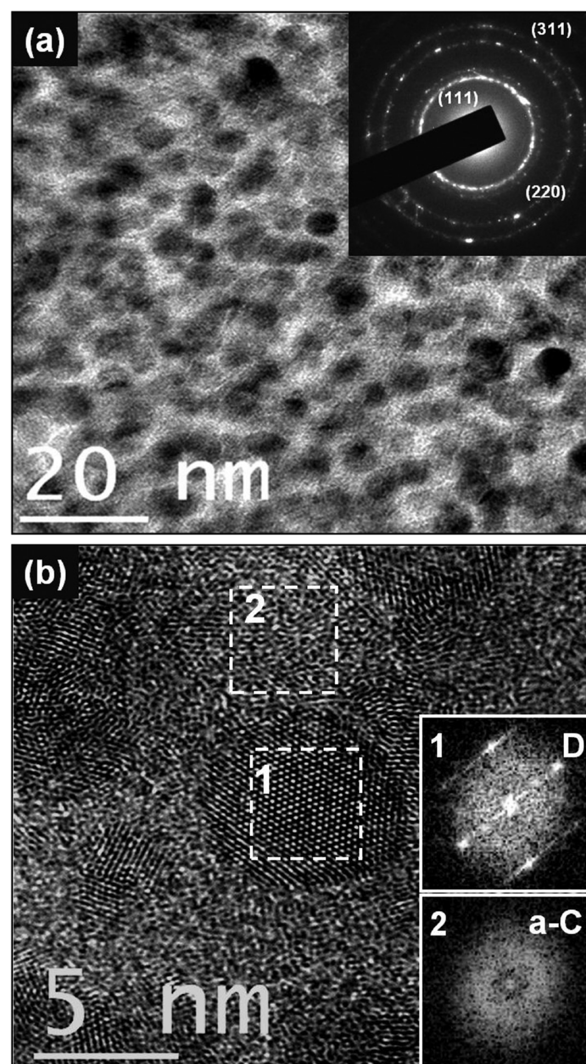

Figure 7. (a) The plane-view TEM micrograph with corresponding SAED pattern shown as inset and (b) structure image with insets 1 and 2 shows the FT images of the regions "1" and "2" of the UNCD/Si films, revealing that films contain equi-axed nanosized diamond grains.

area electron diffraction (SAED) pattern shown in the inset of Figure 7a illustrates that the UNCD grains are of diamond structure. The TEM structure image shown in Figure 7b reveals that the grains are about 5 nm in size and the grain boundaries are of considerable thickness (∼0.1−0.5 nm). The Fourier-transformed (FT) diffractogram corresponding to region "1", shown as the inset 1 in Figure 7b, indicates clearly the diamond phase. In contrast, the grain boundaries (region "2") are of no diffraction contrast, irrespective of the orientation of the samples. Such an observation implies that the grain boundary phases are not crystalline; i.e., they are amorphous. The strong diffused ring in the center of the FT image corresponding to region "2" (inset 2 in Figure 7b) confirms the amorphous nature of the grain boundary regions.

Figure 8a shows a typical cross-sectional TEM micrograph for UNCD/Si, indicating that interface layer is very smooth and sharply defined. The SAED pattern (inset in Figure 8a) shows diffraction rings correspond to the (111), (220), and (311) lattice planes of diamond and the diffused ring corresponds to *a*-C. Figure 8b shows the HRTEM structure image of the

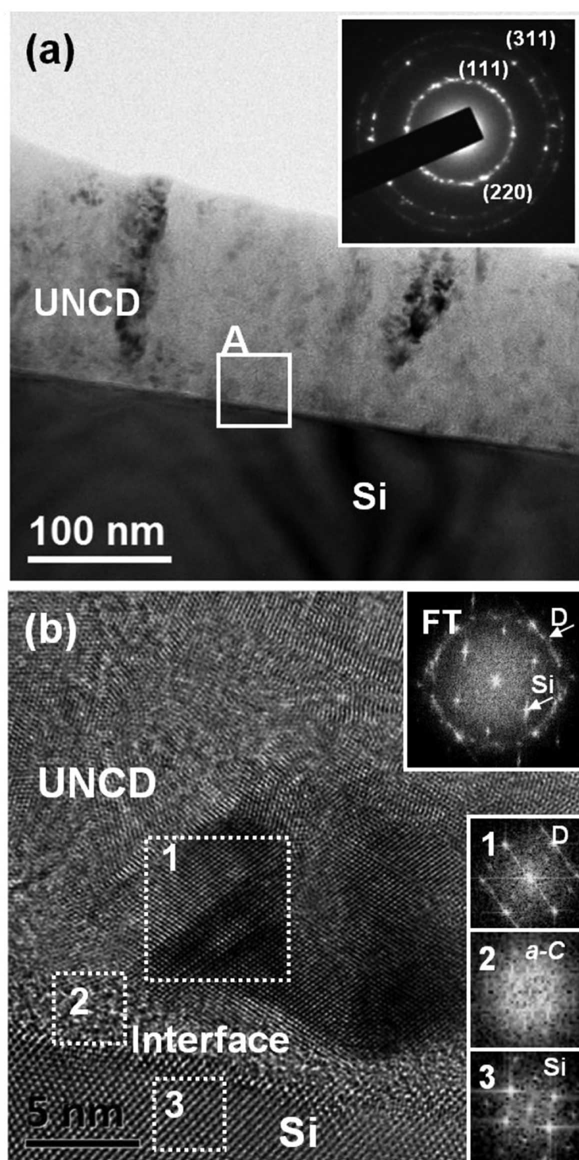

Figure 8. (a) The cross-sectional view TEM micrograph with corresponding SAED pattern shown as inset and (b) cross-sectional structure image (region designated as "A" in panel a) with its FT image shown in the upper right inset. The FT images of selected square regions marked as 1−3 are shown at the lower right of the image for the UNCD/Si films.

region designated as "A" in Figure 8a for UNCD/Si. The upper right inset FT image of Figure 8b shows the typical FT diffractogram for diamond and silicon. The detailed structural investigation using the FT images of regions "'1" and "3" reveals the presence of diamond (FT_1) and silicon (FT_3). In addition, the thin boundary phase between the diamond and Si is illustrated by the FT image of region "2" showing the presence of *a*-*C* (FT_2). Hence, the plane view and cross-sectional view TEM examination of UNCD/Si delivers information to us that there is a thin *a*-*C* phase, existing in the interface between UNCD films and Si and among the nanosized diamond grains. Presumably, this *a*-*C* layer with high electric resistivity hinders the transportation of electrons from substrate to the diamond films, which results in inferior EFE properties for the UNCD/Si films, as compared with those for UNCD/Au−Si films.

In the case of UNCD/Au−Si samples, the modification of their microstructure that enhanced the EFE properties of the films due to Au interlayer is also analyzed using TEM. The low magnified plane-view TEM micrograph shown in Figure 9a

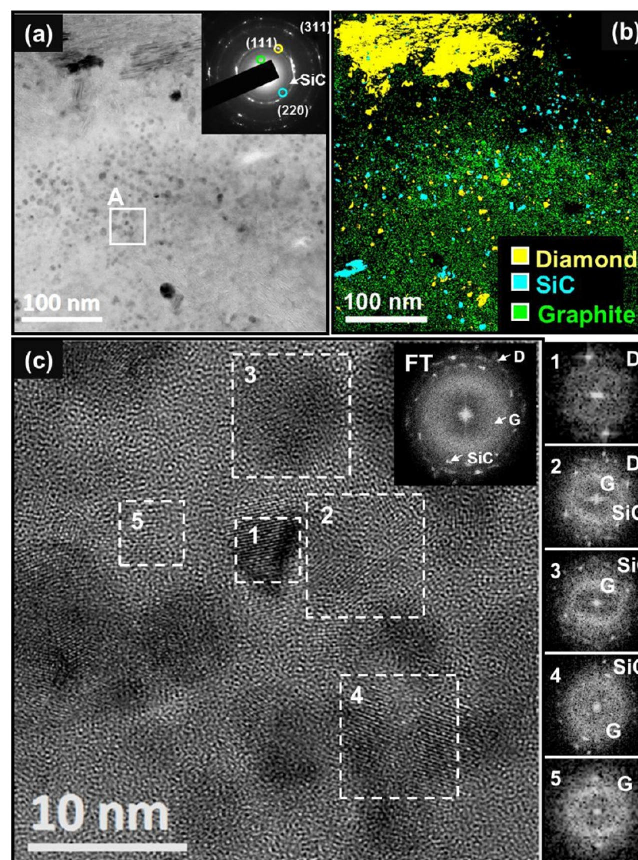

Figure 9. (a) The plane-view TEM micrograph with corresponding SAED pattern shown as inset, (b) HRTEM structure image (region designated as "A" in panel a) with the FT image shown at top right inset. The FT images of selected regions marked as 1−5 are shown at the right side of the image; (c) the composed dark field images corresponding to different spots of SAED (panel a) of the UNCD/Au−Si films.

reveals that the UNCD films contain uniformly nanosized grains with a few aggregates of diamond grains sparsely distributed over the samples. The inset in Figure 9a reveals that the SAED contains mainly the ring shaped pattern, which implies that most of the materials are still randomly oriented nanosized diamond grains. There also exists a prominent diffused ring in the center of this SAED indicating the existence of some graphitic (or *a*-*C*) phase in these films, which is in accord with the Raman spectroscopy observation shown in Figure 5b. It should be noted that there appears a very faint diffraction ring inside the (111) diamond ring that corresponds to (111) SiC phase. The significance of the presence of SiC phase will be further discussed.

More detailed investigations were carried out on the identification of different phase constituents in UNCD/Au−Si films by high resolution TEM studies. Figure 9b shows the structure image for UNCD/Au−Si (designated region "A", Figure 9a). The FT image of the whole structure image shows a spotted diffraction pattern arranged in a ring, which is of diamond (D) phase, and diffused diffraction ring located at the

dx.doi.org/10.1021/am300894u | ACS Appl. Mater. Interfaces 2012, 4, 4169−4176

center of FT image, which corresponds to graphitic (or *a*-C) phase. Moreover, the spotted diffracted inner ring (inside the diamond ring) represents the presence of SiC phase. The FT image corresponding to the region "1" shows the diamond phase. The FT images (FT_2–FT_4) corresponding to the regions marked at 2–4 illustrate more clearly the existence of SiC clusters, which are evenly distributed with the diamond grains and graphitic phases. The FT image, FT_5, corresponding to the region marked 5 illustrates the presence of nanographite phase. Notably, there are graphitic phases coexisting with each of the SiC clusters, as implied by the central diffused patterns in FT_2–FT_4. We also observe that there are some Au grains which are sparsely dispersed in the UNCD/Au–Si films (not shown). To more clearly illustrate the phase constituents of the films, the dark field (DF) images were taken from the diffraction spots corresponding to diamond, graphite, and SiC materials, respectively, and superimposed. Figure 9c shows a typical composed DF image of the UNCD/Au–Si films, revealing that UNCD films contain mostly nanosized grains (yellow color), accompanied with graphite phase (green color). In addition, there exists a SiC phase (blue color), which is evenly distributed among the diamond grains.

Interestingly, the low magnified cross-sectional TEM micrograph of UNCD/Au–Si (Figure 10a) shows that an interface layer of about 15 nm thick is formed above the Au-interlayer and the Au particles are occasionally observed in the interface layer. Diffraction rings from the SAED pattern (inset of Figure 10a) shows the presence of diamond, Au, SiC, and also the graphite phase. Moreover, the cross-sectional HRTEM image of the interface layer (designated region "A", Figure 10a) is shown in Figure 10b. The FT image of the whole structure image (FT) shows that the spotted diffraction pattern arranged in a ring is of diamond (D) phase with the inner spotted ring of SiC phase and diffused diffraction ring located at the center, which matches up to graphitic phase (G). The presence of diamond, SiC, and graphitic phases are highlighted by region "1" (FT_1), region "2" (FT_2), and region "3" (FT_3), respectively. On the basis of these TEM investigations, it is obvious that the formation of SiC clusters and graphitic phases at the interface was enhanced due to the diffusion of Au into the interface layer. Plane-view TEM results show that the UNCD grains are surrounded by graphitic grain boundaries.

From the CITS images (Figure 2b,d), we observed that the grain boundaries are the prominent field emitters in comparison to the grains. These grain boundaries are amorphous for UNCD/Si films and are crystalline nanographite for UNCD/Au–Si films. These nanographitic contained in the grain boundaries of UNCD/Au–Si films form highly conductive channels at the interface of UNCD grain. These channels provide strong field enhancement in the local electric field at the interface, giving rise to prominent electron emission from the grain boundaries. In addition, UNCD/Si films always form *a*-C layer near the UNCD-to-Si interface. This layer of high resistivity hinders the transportation of electrons from substrate to the diamond films and further suppresses the EFE capability. In UNCD/Au–Si films, the diffusion of Au species results in the conducting interfacial layer. The conversion of metal-to-Si interface from resistive to conductive due to Au–Si eutectic reaction also facilitates the electron transportation from the substrate to the surface of diamond films. Hence, the beneficial effect of Au coatings on Si is attributed to the modification of the surface and interface characteristics of the UNCD films and thereafter is enhanced in the field emission properties.

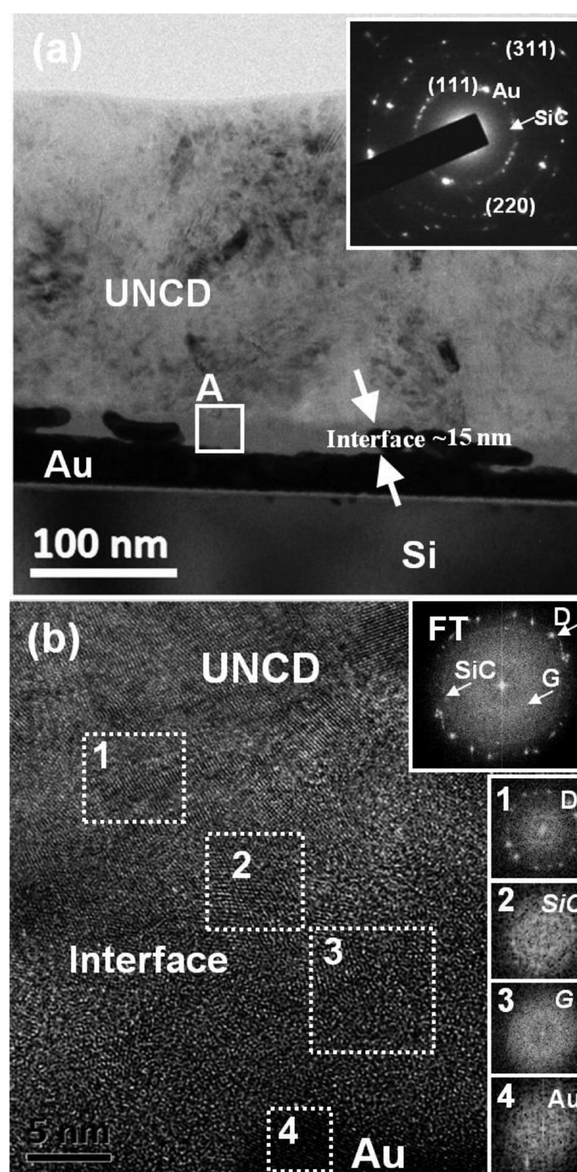

Figure 10. (a) The cross-sectional view TEM micrograph with corresponding SAED pattern shown as inset and (b) cross-sectional structure image (region designated as "A" in panel a) with the FT image shown as top right inset. The FT images of selected square regions marked as 1–4 are shown at the bottom right of the image of the UNCD/Au–Si films.

■ CONCLUSIONS

In summary, the Si and Au-coated Si substrates used in this work do not significantly alter the nucleation and growth behavior of UNCD films but pronouncedly modify the thin film's EFE characteristics. The UNCD/Si films shows low EFE behavior that is ascribed to *a*-C formed in the interface that hinders the transportation of electrons from Si to the UNCD films. Such a difficulty can be circumvented in Au-coated Si substrates. UNCD/Au–Si films possess high conductivity and show superior EFE properties. STM and the *I*–*V* characteristics of STS clearly show distinct features for the diamond grains and grain boundaries present in UNCD/Au–Si substrates. Elec-

dx.doi.org/10.1021/am300894u | ACS Appl. Mater. Interfaces 2012, 4, 4169–4176

tronic band structure estimated by STS measurements reveals a bandgap of 2.8 eV at the grain and shows nearly metallic feature at the grain boundary. STS and CITS measurements show that grain boundaries have higher conductivity and that they are the prominent field emission sites. The plane-view TEM results show that, in the UNCD/Au−Si films, the diamond grains are surrounded by graphitic grain boundaries, which form high conductive channels at the interface of UNCD grains, giving rise to prominent electron emission from the grain boundaries. Moreover, the diffusion of Au in the interface layer results in the introduction of nanographite phases in the interface, lowering the resistivity of the interfacial layer. The electrons can therefore be transferred effortlessly from Si substrates across the interfacial layer to the diamond and can consequently be field emitted. The conducting UNCD/Au−Si films with better EFE characteristics may open up a pathway to the next generation of high-definition flat panel displays or plasma devices.

■ AUTHOR INFORMATION

Corresponding Author

*E-mail: nhtai@mx.nthu.edu.tw.

Notes

The authors declare no competing financial interest.

■ ACKNOWLEDGMENTS

The authors would like to thank the financial support of the National Science Council through the project Nos. NSC 99-2119-M-032-003-MY2 and NSC 98-2221-E-007-045-MY3.

■ REFERENCES

(1) Zhu, W.; Kochanski, G. P.; Jin, S.; Seilbles, L. *J. Appl. Phys.* **1995**, *78*, 2707.
(2) de Heer, W. A.; Chatelain, A.; Ugarte, D. *Science* **1995**, *270*, 1179.
(3) Amaratunga, G. A. J.; Silva, S. R. P. *Appl. Phys. Lett.* **1996**, *68*, 2529.
(4) Sun, M.; Gao, Y.; Zhi, C.; Bando, Y.; Golberg, D. *Nanotechnology* **2011**, *22*, 145705.
(5) Zhai, T.; Fang, X.; Bando, Y.; Dierre, B.; Liu, B.; Zeng, H.; Xu, X.; Huang, Y.; Yuan, X.; Sekiguchi, T.; Golberg, D. *Adv. Funct. Mater.* **2009**, *19*, 2423.
(6) Fan, S.; Chapline, M. G.; Franklin, N. R.; Tombler, T. W.; Cassell, A. M.; Dai, H. *Science* **1999**, *283*, 512.
(7) Shang, N.; Papakonstantinou, P.; Wang, P.; Zakharov, A.; Palnitkar, U.; Lin, I. N.; Chu, M.; Stamboulis, A. *ACS Nano* **2009**, *3*, 1032.
(8) Zhu, W.; Kochanski, G. P.; Jin, S. *Science* **1998**, *282*, 1471.
(9) Geis, M. W.; Efremow, N. N.; Krohn, K. E.; Twichell, J. C.; Lszczarz, T. M.; Kalish, R.; Greer, J. A.; Tabat, M. D. *Nature* **1998**, *393*, 431.
(10) Yamaguchi, H.; Masuzawa, T.; Nozue, S.; Kudo, Y.; Saito, I.; Koe, J.; Kudo, M.; Yamada, T.; Takakuwa, Y.; Okano, K. *Phys. Rev. B* **2009**, *80*, 165321.
(11) Geis, M. W.; Deneault, S.; Krohn, K. E.; Marchant, M.; Lyszczarz, T. M.; Cooke, D. L. *Appl. Phys. Lett.* **2005**, *87*, 192115.
(12) Okano, K.; Koizumi, S.; Silva, S. R. P.; Amaratunga, G. A. J. *Nature* **1996**, *381*, 140.
(13) Watanabe, H.; Nebel, C. E.; Shikata, S. *Science* **2009**, *324*, 1425.
(14) Feng, Z.; Brown, I. G.; Ager, J. W. *J. Mater. Res.* **1995**, *10*, 1585.
(15) Zhu, W.; Kochanski, G. P.; Jin, S.; Seibles, L. *J. Appl. Phys.* **1995**, *78*, 2707.
(16) Geis, M. W.; Twichell, J. C.; Lyszczarz, T. M. *J. Vac. Sci. Technol. B* **1996**, *14*, 2060.
(17) Corrigan, T. D.; Gruen, D. M.; Krauss, A. R.; Zapol, P.; Chang, R. P. H. *Diamond Relat. Mater.* **2002**, *11*, 43.
(18) Pradhan, D.; Lin, I. N. *ACS Appl. Mater. Interfaces* **2009**, *1*, 1444.
(19) Birrell, J.; Carlisle, J. A.; Auciello, O.; Gruen, D. M.; Gibson, J. M. *Appl. Phys. Lett.* **2002**, *81*, 2235.
(20) Lin, Y. C.; Sankaran, K. J.; Chen, Y. C.; Lee, C. Y.; Chen, H. C.; Lin, I. N.; Tai, N. H. *Diamond Relat. Mater.* **2011**, *20*, 191.
(21) Teng, K. Y.; Chen, H. C.; Chiang, H. Y.; Horng, C. C.; Cheng, H. F.; Sankaran, K. J.; Tai, N. H.; Lee, C. Y.; Lin, I. N. *Diamond Relat. Mater.* **2012**, *24*, 188.
(22) Mandel, Th.; Frischholz, M. *Appl. Surf. Sci.* **1993**, *65*, 795.
(23) Xu, N. S.; Tzeng, Y.; Latham, R. V. *J. Phys. D* **1993**, *26*, 1776.
(24) Nemanich, R. J.; Bergman, L. *Phys. B* **1993**, *185*, 528.
(25) Wolter, S. D.; Stoner, B. R.; Glass, J. T.; Ellis, P. J.; Buhaenko, D. S.; Jenkin, C. E.; Southworth, P. *Appl. Phys. Lett.* **1993**, *62*, 1215.
(26) Stoner, B. R.; Sahaida, S. R.; Bade, J. P.; Southworth, P.; Ellis, P. J. *J. Mater. Res.* **1993**, *8*, 1334.
(27) Bhusari, D. M.; Yang, J. R.; Wang, T. Y.; Chen, K. H.; Lin, S. T.; Chen, L. C. *Mater. Lett.* **1998**, *36*, 279.
(28) Shen, M. R.; Wang, H.; Ning, Z. Y.; Ye, C; Gan, Z. Q.; Ren, Z. X. *Thin Solid Films* **1997**, *301*, 77.
(29) Michau, D.; Tanguy, B.; Demazeau, G.; Coizi, M.; Cavagnat, R. *Diam. Relat. Mater.* **1993**, *2*, 19.
(30) Gu, C. Z. *Appl. Surf. Sci.* **2005**, *251*, 225.
(31) Jiang, N.; Nishimura, K.; Shintani, Y.; Hiraki, A. *J. Cryst. Growth* **2003**, *255*, 102.
(32) Hugues, A. G.; Sandrine, P.; Celine, G.; Marc, C.; Laetitia, V.; Jean, C. A.; Philippe, B.; Jean, P. B.; Thierry, G. *ACS Appl. Mater. Interfaces* **2009**, *1*, 2738.
(33) Amelie, V.; Thomas, G.; Zhi, Q. X.; Craig, A. Z.; Dennis, R. A.; Jean, F. S.; Jean, M. H.; Namas, C.; Yong, F. L. *ACS Appl. Mater. Interfaces* **2011**, *3*, 1134.
(34) Groning, O.; Nilsson, L. O.; Groning, P.; Schlapbach, L. *Solid-State Electron.* **2001**, *45*, 929.
(35) Dubray, J. J.; Pantano, C. G.; Meloncelli, M.; Bertran, E. *J. Vac. Sci. Technol., A* **1991**, *9*, 3012.
(36) Meilunas, R. J.; Chang, R. P. H.; Kiu, S.; Kappes, M. M. *Appl. Phys. Lett.* **1991**, *59*, 3461.
(37) Chen, H. C.; Liu, K. F.; Tai, N. H.; Pong, W. F.; Lin, I. N. *Diamond Relat. Mater.* **2010**, *19*, 134.
(38) Silva, F. J. G.; Baptista, A. P. M.; Pereira, E.; Teixeira, V.; Fan, Q. H.; Fernandes, A. J. S.; Costa, F. M. *Diamond Relat. Mater.* **2002**, *11*, 1617.
(39) Pradhan, D.; Chen, L. J.; Lee, Y. C.; Tai, N. H.; Lin, I. N. *Diamond Relat. Mater.* **2006**, *15*, 1779.
(40) Chen, L. J.; Tai, N. H.; Lee, C. Y.; Lin, I. N. *J. Appl. Phys.* **2007**, *101*, 064308.
(41) Li, Y. S.; Tang, Y.; Yang, Q.; Maley, J.; Sammynaiken, R.; Regier, T.; Xiao, C.; Hirose, A. *ACS Appl. Mater. Interfaces* **2010**, *2*, 335.
(42) Luo, J. Y.; Liu, K. S.; Lee, J. S.; Lin, I. N.; Cheng, H. F. *Diamond Relat. Mater.* **1998**, *7*, 704.
(43) Lee, J. S.; Liu, K. S.; Lin, I. N. *J. Appl. Phys.* **1997**, *82*, 3310.
(44) Fowler, R. H.; Nordheim, L. *Proc. R. Soc. London, Ser. A* **1928**, *119*, 173.
(45) Feenstra, R. M. *Surf. Sci.* **1994**, *299*, 965.
(46) Feenstra, R. M.; Martensson, P. *Phys. Rev. Lett.* **1988**, *61*, 4.
(47) Williams, O. A.; Curat, S.; Gerbi, J. E.; Gruen, D. M.; Jackman, R. B. *Appl. Phys. Lett.* **2004**, *85*, 1680.
(48) Lud, S. Q.; Niedermeier, M.; Koch, P. S.; Bruno, P.; Gruen, D. M.; Stutzmann, M.; Garrido, J. A. *Appl. Phys. Lett.* **2010**, *96*, 092109.
(49) Sasagawa, T.; Shen, Z. X. *J. Appl. Phys.* **2008**, *104*, 073704.
(50) Ferrari, A. C.; Robertson, J. *Phys. Rev. B* **2001**, *63*, 121405.
(51) Corrigan, T. D.; Gruen, D. M.; Krauss, A. R.; Zapol, P.; Chang, R. P. H. *Diamond Relat. Mater.* **2002**, *11*, 43.
(52) Ferrari, A. C.; Robertson, J. *Phys. Rev. B* **2000**, *61*, 14095.
(53) Kalish, R. *Carbon* **1999**, *37*, 781.
(54) Ilie, A.; Ferrari, A. C.; Yagi, T.; Rodil, S. E.; Robertson, J.; Barborini, E.; Milani, P. *J. Appl. Phys. D* **2003**, *36*, 2001.